

Deep Learning-Based Blind Multiple User Detection for Grant-free SCMA and MUSA Systems

Thushan Sivalingam, *Graduate Student Member, IEEE*, Samad Ali, *Member, IEEE*, Nurul Huda Mahmood, *Member, IEEE*, Nandana Rajatheva, *Senior Member, IEEE*, and Matti Latva Aho, *Senior Member, IEEE*

Abstract

Grant-free random access and uplink non-orthogonal multiple access (NOMA) are techniques to increase the overload factor and reduce transmission latency with signaling overhead in massive machine-type communications (mMTC). Sparse code multiple access (SCMA) and Multi-user shared access (MUSA) are introduced as advanced code domain NOMA schemes. In grant-free NOMA, machine-type devices (MTD) transmit information to the base station (BS) without a grant, creating a challenging task for the BS to identify the active MTD among all potential active devices. In this paper, a novel deep neural network (DNN)-based multi-user detection (MUD) scheme for the grant-free SCMA and MUSA system in an mMTC uplink framework is proposed to jointly identify the received signal's sparsity and the active MTDs in the absence of channel state information. The proposed scheme learns the correlation between the received signal and the multi-dimensional codebook for SCMA and spreading sequences for MUSA schemes and is able to identify the active MTDs from the received signal without any prior knowledge of the device sparsity level. The application of the proposed MUD scheme is further investigated in an indoor factory setting using four different mmWave channels. Numerical results show that when the number of active MTDs in the system is large, DNN-MUD has a significantly higher probability of detection compared to existing approaches over the signal-to-noise ratio range of interest.

Index Terms

Deep neural network, grant-free, machine-type communications, multi-label classification, multi-user detection, MUSA, ResNet, SCMA, NOMA.

This work was supported by the Academy of Finland 6Genesis Flagship (grant no. 318927). This article was presented in part at the IEEE PIMRC 2021 [1], [2].

I. INTRODUCTION

Massive machine-type communications (mMTC) is foreseen as one of the leading service classes for sixth-generation (6G) wireless communication systems [3]. mMTC supports a wide range of industrial, medical, commercial, defense, and general public applications in the Internet-of-Things domain. mMTC focuses on supporting the uplink-dominated massive number of low-power and low-complexity devices that sporadically transmit short data packets [4] with low transmission rates during the short period of the active state. Therefore the conventional four-step scheduling-based multiple access schemes in which the base station (BS) allocates orthogonal time/frequency resources to each device are inefficient because of the heavy signaling overhead and higher access delay [5].

A. *State-of-the-art*

Grant-free non-orthogonal multiple access (NOMA) schemes have been proposed as a promising solution [6] to overcome the above-mentioned limitations. Grant-free access allows the machine-type devices (MTDs) to communicate pilot and information symbols without acquiring a transmission grant, thereby significantly reducing the signaling overhead. NOMA techniques have been extensively investigated to potentially support a massive number of MTDs by sharing a limited amount of time and frequency resources in a non-orthogonal manner [6]. In this approach, there is inter-user interference because of the orthogonality violation. Therefore, NOMA applies device-specific non-orthogonality sequences to mitigate the inter-user interference [6]. In this regard, several signature-based NOMA schemes were proposed based on device-specific codebook structures, interleaving patterns, delay patterns, scrambling sequences, and spreading sequences [7]. From this perspective, the sparse coded multiple access (SCMA) is designed as a code-domain-NOMA technique [8] by Huawei, and multi-user shared access (MUSA) is introduced by ZTE [9] as a spreading-sequence-based NOMA scheme.

Recognizing the underlying challenge of grant-free access that each MTD transmits information without scheduling, a mechanism is required at the BS to detect the active MTDs among all inherent devices in the network. This procedure is defined as multi-user-detection (MUD). In mMTC network, a single MTD is not active for a long period, and only a few devices are active in a particular time frame. Due to the infrequent nature of mMTC traffic, the activity vector, which marks the active devices out of all available MTDs, can be represented as a sparse vector. This problem can be formulated as a sparse signal recovery problem by considering the

sparsity of the activity vector. Furthermore, based on the antenna configuration of the BS, this problem can be regarded as a single measurement vector (SMV) MUD problem where BS has a single antenna or multiple measurement vector (MMV) MUD problem where BS has multiple antennas. Solving this problem involves two subqueries, i) how many devices are active and ii) which are those active devices.

A number of studies based on compressive sensing (CS) theory have recently been proposed to exploit the sparse characteristic of device activity [10]–[14]. The study [10] proposes a maximum a posteriori probability (MAP) based approach to identify active devices and their corresponding data symbols simultaneously. The authors in [11] proposed a generalized MMV based CS-approximate message passing (AMP) algorithm for joint active user detection (AUD) and channel estimation (CE) by considering the sporadic traffic nature and the virtual angular domain sparsity of massive multiple input multiple outputs (MIMO) channels. The work in [12] investigates the structured sparsity of the active users and proposes a low-complex structured CS-based iterative algorithm to detect the active users and data jointly. To improve the MUD performance, the authors in [13] propose a prior-information-aided adaptive subspace pursuit (PIA-ASP) algorithm to exploit the intrinsically temporal correlation of active user support sets in several continuous-time slots. Moreover, dynamic CS-based MUD proposed in [14] to detect both active users and their corresponding data jointly in several continuous-time slots by exploring the temporal correlation of the active user sets. In addition, the designers of SCMA and MUSA started the ball rolling on blind MUD [15], [16]. Reference [15] proposes an iterative algorithm to detect the active pilots and decoding mechanism of user's data. In [16], the authors present MUD without the reference signal at the BS for MUSA. First, the spreading codes used by the active users are estimated by an iterative algorithm. Then the active users are detected by blind equalization.

With a high overloading ratio (OR) where the number of devices is higher than the number of resources, the performance of the previously mentioned [10]–[16] CS-based approaches degrade due to the increased correlation between the columns of the sensing matrix. Furthermore, the performance degradation would be high when the sparsity of the input vector increases in mMTC. Besides, conventional CS-based solutions strongly depend on the channel estimation quality. However, perfect channel estimation cannot be accomplished in practical mMTC. The aforementioned iterative algorithms also take a considerable amount of time to converge, which increases the communication latency. Even though a significant amount of literature has been published based on conventional algorithms, those literature have not entirely addressed the

realistic nature of the MUD for mMTC. Taken together, developing a practically feasible, scalable MUD scheme for grant-free SCMA and MUSA for mMTC is a challenging open problem.

Cutting-edge explorations and expansions of machine learning have started to address critical problems in wireless communication driven by the advancement of computational capabilities and algorithm complexities [17]. In this viewpoint, two studies have attempted to explore the MUD problem by deep learning, e.g., [18], [19]. Both studies propose MUD for a grant-free low-density signature (LDS) scheme. In [18], the authors present deep learning-based parallel receivers with a softmax estimator for each distinct sparsity level. However, sparsity estimation based on softmax thresholding performs better only for specific sparsity levels where the pre-defined threshold value satisfies the estimation conditions. Furthermore, designing a distinct MUD strategy for each sparsity level is impractical, and it limits the algorithm's scalability. From a theoretical point of view, softmax takes the value of the layer before and produces a probability distribution, where output values are interrelated. Also, the initial problem formulation consists of independent devices; therefore, using softmax is not a proper approach. Moreover, depending ensemble learning has a risk of carrying a high bias toward its aggregate and is undoubtedly expensive in computational and implementation complexity. In the study [19] the authors fix the number of active devices during the training, which does not enable deep neural networks (DNN) to learn the entire codebook of the network. Therefore, it induces misdetection during practical implementation. These approaches as given [18], [19] are unsatisfactory because they did not wholly consider realistic mMTC scenarios and deep learning design criteria. Consequently, there is a need to develop a practically feasible deep learning-based MUD for the SCMA and MUSA schemes.

B. Contribution

The major contributions of this study are as follows:

- We propose a novel pre-activated residual neural network (ResNet)-based blind DNN-MUD architecture for two different grant-free NOMA schemes: SCMA codebooks and MUSA spreading sequences with diverse ORs. Our proposed architecture learns the correlation between the received signal and the device-specific codebooks for SCMA and spreading sequences for MUSA during the offline training, further jointly detecting the received signal's sparsity and corresponding active devices by a sigmoid estimation online without channel state information (CSI).

- We formulate a SMV sparse signal recovery problem for jointly achieving sparsity and active devices. Further, we re-structure the received measurement vector by separating the real and imaginary components and stacking them as an input vector to construct the training data while annotating the status of the MTDs to generate the training labels. This training data and corresponding labels are given to the DNN to learn the internal parameters, including the codebook and spreading sequence entries and combinations of the active devices in the mMTC system.
- Since there are no readily available SCMA codebooks and MUSA spreading sequences for massive devices, we design SCMA codebooks for different ORs with constellation rotation and interleaving based on [8], [20] and generate a feasible set of MUSA spreading sequences based on [9]. However, it is challenging to choose the best MUSA spreading sequences from the available set; therefore, we propose a scalable heuristic algorithm to determine the spreading sequences with the required orthogonality factor among the potential set to reduce the correlation between the MUSA spreading codes.
- We further expand our DNN algorithm to address the MUD of the MMV system, where we separate the real and imaginary elements of each antenna measurement and serially stack them to construct the input training data. However, we use the same SMV technique to annotate the training labels.
- We broadly evaluate the proposed DNN-MUD performance with a comparison of existing well-known algorithms such as least squares-block orthogonal matching pursuit (LS-BOMP) [21], complex-AMP (C-AMP) [22], and stagewise orthogonal matching pursuit (stOMP) [23] algorithms. Also, we examine the SMV scenario for the mmWave indoor factory environment [24] to validate the performance of the DNN-MUD in realistic circumstances.
- We derive the computational complexity of the proposed DNN-MUD architecture and provide the complexity of the previously mentioned well-known algorithms to compare the collective effectiveness with MUD.

The structure of our paper is as follows. Section II presents the system model and problem formulation, including the concept, generation, and code selection of SCMA codebook and MUSA spreading sequences. Section III describes the deep learning approach and MUD structure for SMV and MMV systems. Section IV shows the complexity, training, and testing data

generation. Section V presents the simulation setup, parameters, and numerical results. Finally, Section VI concludes the study.

Notations: Boldface uppercase, boldface lowercase, and lower case letters represent matrices, vectors, and scalars, respectively, whereas calligraphy letters denote sets. \mathbb{R} and \mathbb{C} denote the space of real and complex numbers, respectively. The operations $(\cdot)^H$ and $(\cdot)^T$ denote conjugate transpose and transpose, respectively. $\Re(s)$ and $\Im(s)$ are the real and imaginary part of a complex number s , respectively. \mathbf{I} denotes the identity matrix, where the size is evident from the context. In addition, complex Gaussian distribution with zero mean, and variance σ_w^2 is represented by $\mathcal{CN}(0, \sigma_w^2)$. The Hadamard (element-wise) product operator is denoted by \circ . Also, the absolute value of the complex number x is represented by $|x|$ and Euclidean norm of the vector \mathbf{x} is denoted by $\|\mathbf{x}\|$.

II. SYSTEM MODEL AND PROBLEM FORMULATION

A. System Model

Consider the uplink grant-free NOMA system of a mMTC network where a set \mathcal{N} of N randomly distributed MTDs are served by a BS. In the SMV scenario, the BS and MTDs are each equipped with a single antenna, and in the MMV scenario, the BS is equipped with multiple antennas, and MTDs are equipped with a single antenna. In this study, we focus on the overloaded scenario, where the number of MTDs is higher than the available uplink radio resources K ($K < N$) and OR $\triangleq N/K$. Each MTD operates independently in this network. Furthermore, only a small subset of MTDs is active n out of N at any given time; the rest of the MTDs are inactive, shown in Fig. 1. We consider a slotted time access mechanism where the active MTDs at a given time slot access the medium synchronized in time. All active MTDs communicate to the BS after spreading with the device-specific non-orthogonal codebook in SCMA and non-orthogonal complex spreading sequences in MUSA schemes. Since each active MTDs share information spontaneously without scheduling, the BS needs to classify the active MTDs, i.e., determine the number of active devices, their identity, and transmitted data.

B. Problem Formulation

We define the binary state indicator (active or inactive) a_i of the i -th MTD as

$$a_i = \begin{cases} 1, & \text{ith MTD is active,} \\ 0, & \text{ith MTD is inactive.} \end{cases} \quad (1)$$

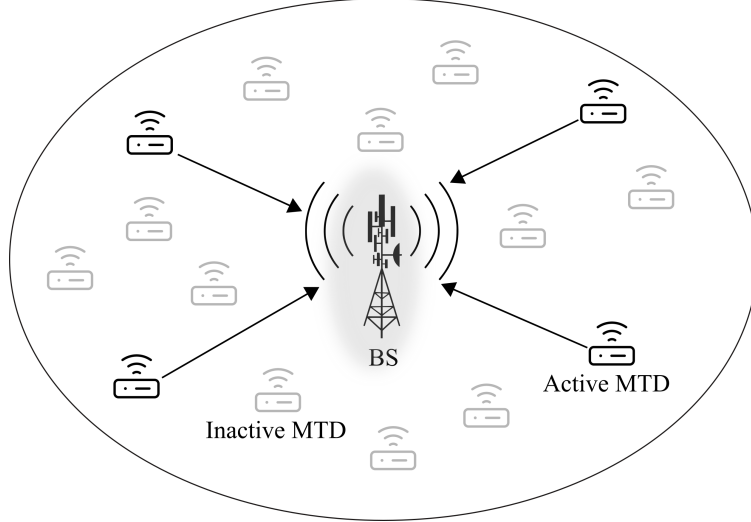


Fig. 1: The illustration of mMTC grant-free NOMA uplink communication system where a fraction of devices transmits information to the BS.

The probability of the active state of the i -th MTD is p_i , which is independent of other devices in the cell. The received signal $\mathbf{y} \in \mathbb{C}^K$ at the BS can be expressed as

$$\mathbf{y} = \sum_{i=1}^N a_i \mathbf{s}_i h_i x_i + \mathbf{w}, \quad (2)$$

where $\mathbf{s}_i \in \mathbb{C}^K$ is the spreading sequence vector of the i -th MTD (device specific codeword vector for SCMA and complex spreading sequence for MUSA), h_i is the complex uplink channel coefficient from the i -th MTD to the BS which includes both small and distance-dependent large scale fading, x_i is the transmit symbol of the i -th MTD, and $\mathbf{w} \in \mathbb{C}^K \sim \mathcal{CN}(0, \sigma_w^2 \mathbf{I})$ is the complex-Gaussian noise vector. As specified earlier, at the beginning of the transmission, BS does not have knowledge of the number of active devices and corresponding spreading sequences. Therefore BS performs MUD to identify them. In particular, all the active MTDs transmit the pilot symbol $x_{p,i}$ to the BS in order to assist it to detect the active devices and corresponding spreading sequences (\mathbf{s}_i). After that, it estimates the channel coefficients (h_i). Finally, BS decodes the J data symbols $x_{d,i}^{[1]}, \dots, x_{d,i}^{[J]}$ transmitted by the active MTDs. The transmission is over $J+1$ slots, where J is selected such that the channel coherence time is greater than the transmission time of $J+1$ transmission slots. The pilot measurement vector $\mathbf{y}_p \in \mathbb{C}^K$ is given by

$$\mathbf{y}_p = \sum_{i=1}^N a_i \mathbf{s}_i h_i x_{p,i} + \mathbf{w}. \quad (3)$$

Let us define $\phi_i = \mathbf{s}_i x_{p,i}$, and $\Phi = [\phi_1, \dots, \phi_N]$, we then have

$$\mathbf{y}_p = \sum_{i=1}^N \phi_i a_i h_i + \mathbf{w} = \Phi(\mathbf{a} \circ \mathbf{h}) + \mathbf{w}, \quad (4)$$

where $\mathbf{a} = [a_1, \dots, a_N]^T$ is the activity vector, and $\mathbf{h} = [h_1, \dots, h_N]^T$ is the channel vector. Let us define $\varphi = (\mathbf{a} \circ \mathbf{h}) = [a_1 h_1, \dots, a_N h_N]^T$. We can rewrite (4) as

$$\mathbf{y}_p = \Phi \varphi + \mathbf{w}. \quad (5)$$

We consider a fraction of MTDs (n out of N) to be active at any given time. The accumulated sparse vector φ has n non zero elements. Therefore, the received vector \mathbf{y}_p can be represented as a linear combination of n submatrices of $\phi_1 \dots \phi_N$ perturbed by the noise. There is an essential difference in the formulation of this problem for both SCMA and MUSA schemes. The actual code assignments for the two systems are different from each other. In SCMA schemes, BS knows the device-specific non-orthogonal codebook for each MTD. Therefore, Φ is available at the BS. The main task of the BS is to identify the m submatrices in the received vector. For example, if the first and the third devices are active, then ϕ_1 and ϕ_3 are the components of \mathbf{y}_p . In MUSA sequence-based NOMA schemes, each MTD can choose the spreading sequences independently, which eases the resource coordination of the BS. However, BS knows all the available spreading sequences and pilot symbols. Consequently, the objective of MUD at the BS in MUSA scheme is to detect the n submatrices in the received signal vector. For instance, if the second and the third codes are taken by active MTDs, then ϕ_2 and ϕ_3 are the components of \mathbf{y}_p . Hence, the MUD problem can be formulated as the sparse signal recovery problem:

$$\Omega = \arg \min_{|\Omega|=n} \frac{1}{2} \| \mathbf{y}_p - \Phi_{\Omega} \varphi_{\Omega} \|_2^2. \quad (6)$$

C. Codebook-SCMA

SCMA is designed as a non-orthogonal multi-dimensional structured codebook with layer-specific shaping gain where shaping gain is achieved by utilizing the QAM modulation [25]. The fundamental approach of SCMA is directly mapping the incoming MTD's bits into a codeword vector, where bit to symbol mapping and spreading are coupled together. Furthermore, SCMA codewords are sparse, whereas the non-zero entries in the codeword are the assigned orthogonal channel resources for the uplink communication to the specific MTD [26]. The number of non-zero elements in the codeword is defined as a diversity order of the codeword. Moreover, the

same diversity order assigns for different devices. In this work, we design the codebooks based on [8], [20]. The design includes constellation rotation and interleaving. The multi dimensional SCMA codebook of i -th MTD device $\mathbf{S}_i \in \mathbb{C}^{K \times R}$ is defined as

$$\mathbf{S}_i = \mathbf{V}_i \Delta_i \mathbf{M}_c, \text{ for } i = 1, 2, \dots, N, \quad (7)$$

where R is the constellation points, $\mathbf{V}_i \in \mathbb{B}^{K \times U}$ is the U -dimensional SCMA binary mapping matrix of i -th MTD, Δ_i is the constellation operator of the i -th MTD, and \mathbf{M}_c is the mother constellation. The matrix \mathbf{V}_i can be generated by including $K - U$ all-zero row vectors inside the rows of \mathbf{I}_U [8]. Furthermore, the SCMA design contains the properties below: $N = \binom{K}{U}$ and number of MTDs connected to the same resource, $d_f = \binom{K-1}{U-1}$. Details of Δ_i and \mathbf{M}_c are described in the below subsections. The design of SCMA consists of two major parts, designing the multi-dimensional mother codebook and constructing the codebook based on the number of MTDs.

1) *Design of SCMA mother codebook:* First, two-dimensional lattice (\mathbb{Z}^2) with R points is defined as the first dimension of the mother constellation, where the steps of the design and theory of the lattice constellation are described in [8]. Then, we perform the Gray mapping for each element in the first dimension set. After that, the remaining required number of dimensions is generated using the first dimension's rotation with the corresponding Gray mapping, which gives us the complete mother constellation. However, this constellation is not efficient enough to control the effect of channel fading [20]. Therefore, to improve the energy efficiency of the codeword and reduce the peak to average power ratio, the authors in [20] propose to use interleaving. Furthermore, they claimed that this interleaving could improve the performance in the fading channels. During interleaving, even rows of the initial constellation are reordered as given in [20] while the odd rows are kept as before, which provides us with the final mother constellation (\mathbf{M}_c).

2) *Generation of factor graph for a separate codebook:* The next step is to construct a device-specific codebook for each MTD. Two significant conditions must be followed while constructing the device-specific codeword, such as retaining the Euclidian distance profile and structure of the mother codebook. The authors in [8], [20] propose to use Latin square and factor graph-based constellation to ensure the conditions. The factor graph representation describes the relation between the MTDs and the resource elements. The factor graph matrix of this system described as $\mathbf{F} = (\mathbf{f}_1, \dots, \mathbf{f}_N)$, where each vector (\mathbf{f}_i) contains 1s and 0s. The elements of the

vector, (\mathbf{f}_i) assigned based on U , and d_f where there are U non-zero elements in each column and d_f number of non-zero elements in each row in the \mathbf{F} matrix. Factor graph matrix for $N = 8$, $K = 6$, $U = 3$, and $d_f = 4$ given for example as

$$\mathbf{F} = \begin{bmatrix} 1 & 1 & 1 & 1 & 0 & 0 & 0 & 0 \\ 0 & 0 & 0 & 0 & 1 & 1 & 1 & 1 \\ 0 & 1 & 0 & 0 & 0 & 1 & 1 & 1 \\ 1 & 0 & 1 & 1 & 1 & 0 & 0 & 0 \\ 0 & 1 & 0 & 0 & 0 & 1 & 1 & 1 \\ 1 & 0 & 1 & 1 & 1 & 0 & 0 & 0 \end{bmatrix}. \quad (8)$$

Next, we replace the d_f non-zero elements of each row of the factor graph matrix \mathbf{F} with each of the d_f phase rotation angles ϱ_i according to the Latin structure. This ensures that the any given phase rotation angle does not appear twice within the same row or column. The phase rotation angle ϱ_i is defined as [27]

$$\varrho_i = \exp \left(j \frac{2\pi}{Rd_f} (i-1) \right), i = 1, 2, \dots, d_f. \quad (9)$$

As an example, for $d_f = 4$, the phase rotation angles will be $(\varrho_1, \varrho_2, \varrho_3, \varrho_4)$, and the corresponding updated factor graph matrix is

$$\tilde{\mathbf{F}} = \begin{bmatrix} \varrho_1 & \varrho_2 & \varrho_3 & \varrho_4 & 0 & 0 & 0 & 0 \\ 0 & 0 & 0 & 0 & \varrho_1 & \varrho_2 & \varrho_3 & \varrho_4 \\ 0 & \varrho_3 & 0 & 0 & 0 & \varrho_4 & \varrho_1 & \varrho_2 \\ \varrho_4 & 0 & \varrho_1 & \varrho_2 & \varrho_3 & 0 & 0 & 0 \\ 0 & \varrho_4 & 0 & 0 & 0 & \varrho_1 & \varrho_2 & \varrho_3 \\ \varrho_3 & 0 & \varrho_4 & \varrho_1 & \varrho_2 & 0 & 0 & 0 \end{bmatrix}. \quad (10)$$

Finally, the device-specific constellation operator $\triangle_i \in \mathbb{C}^{U \times U}$ for i -th MTD can be define as

$$\triangle_i = \text{diag}(\tilde{\mathbf{f}}_i), \quad (11)$$

where $\tilde{\mathbf{f}}_i$ is the i -th column of the updated factor graph matrix $\tilde{\mathbf{F}}$ without zero entries.

D. Spreading sequence-MUSA

MUSA spreading sequences are designed to support massive MTDs in a dedicated amount of radio resources. In the MUSA scheme, each MTD information is spread with a group of low cross-correlation complex spreading sequences. BS can generate a large set of possible

MUSA codes with specific M -ary values and required code lengths (number of radio resources). Also, MUSA codes are designed to support high OR with small code lengths to handle power consumption and delay efficiently. Furthermore, the different M -ary values and code length define the space of available MUSA sequences [9]. MUSA considers the independence of choosing real and imaginary parts of the complex spreading elements; it has the feasibility to select from $M = 2$, where the set $\{1, -1\}$ is considered as binary sequences. It can produce only 4 elements $\{-1 + i, -1 - i, 1 + i, 1 - i\}$, which may not provide sufficient freedom to choose the required amount of codes for mMTC. Moreover $M = 3$ codes are generated from the basic element set $\{-1, 0, 1\}$. Then the complex spreading elements are generated from the basic element set, for example $\{-1 + i, -1, -1 - i, i, 0, -i, 1 + i, 1, 1 - i\}$ is the possible complex element set for $M = 3$ codes. We consider only $M = 3$ codes for our study, which is recommended by the MUSA designers [9] and able to produce an adequate amount of codes.

After generating the complex spreading elements, we can create the space of all possible MUSA sequences by permuting them according to the required code length. Therefore, the set \mathcal{M} of 9^K complex sequences can be generated from $M = 3$ codes. However, we need only N number of MUSA spreading sequences. Out of all available sequences, some are highly cross-correlated sequences, which reduces the MUD performance. Rather than randomly choosing N columns of the all possible MUSA sequence, we propose a scalable heuristic algorithm to choose a required number of low-cross correlated sequences, which is summarised in Algorithm 1. Given a cross-correlation threshold ρ , the proposed algorithm selects a subset $\tilde{\mathcal{M}}$ of \mathcal{M} , such that the mutual cross-correlation between any two elements of $\tilde{\mathcal{M}}$ is less than or equal to ρ .

III. DEEP LEARNING-BASED MUD AND SPARSITY ESTIMATION

A. Proposed Solution Approach

This study aims to pave the way for the practical implementation of mMTC traffic MUD under the grant-free access scheme. Considering the sporadic nature of MTD activation pattern in mMTC traffic, only a small subgroup of the entire group of MTDs is active in a given time. By employing this fact, the MUD problem can be expressed as a deep learning-based multi-label classification. As the name suggests, multi-label classification detects the mutually non-exclusive multiple labels associated with the single data. In our problem, the labels are active and inactive states of the MTDs, and data is the received signal at the BS.

Algorithm 1: A heuristic algorithm to select low-cross correlated MUSA sequences

Input: Cross-correlation threshold ρ

Output: A matrix $\tilde{\mathcal{M}}$ of MUSA sequences with low mutual cross-correlation

Data: Matirx \mathcal{M} with all possible combination of MUSA sequences

1 **Initialization:** Candidate columns $\mathcal{C} = \mathcal{M}; \tilde{\mathcal{M}} = \emptyset;$

2 **while** \mathcal{C} **do**

3 \mathbf{m} = randomly selected column from \mathcal{C} ;

4 $\tilde{\mathcal{M}} = \tilde{\mathcal{M}} \cup \mathbf{m};$

5 $\mathcal{C} = \left\{ \mathbf{c} \mid \mathbf{c} \in \mathcal{C}, \left(\frac{\mathbf{c}}{\|\mathbf{c}\|} \right)^T \left(\frac{\mathbf{m}}{\|\mathbf{m}\|} \right) \leq \rho \right\}$

The objective of the DNN-based MUS is to detect the corresponding labels of the φ . Here, the number of labels and their positions will be the number of active devices and their codebooks for SCMA and spreading sequences for MUSA. Therefore, we are not focusing on the recovery of the nonzero components. A major advantage of our proposed scheme is that since we train our network with sufficient training data, we do not need to estimate the channel before the detection. Therefore, we introduce a ResNet-based architecture to solve the above-mentioned tasks jointly. This architecture consists of several hidden nodes connecting the input layer to the output layer. Here each data item from the training data (\mathbf{y}_p) set is tagged with the corresponding label (ψ). In order to solve the two subtasks, the proposed model learns the mapping function associating the input nodes and related labels by updating the hidden parameters using the backpropagation process. Clearly, It is the nonlinear mapping g between \mathbf{y}_p and sparse vector elements of φ . Subsequently, we reformulate the problem (6) as

$$\Omega = g(\mathbf{y}_p; \omega, \theta), \quad (12)$$

where ω is the set of weights of the hidden layers, and θ is the set of biases of the hidden layers of the neural network. The explicit intention of this DNN-MUD is to obtain g characterized by ω and θ given \mathbf{y}_p , nearest to the unknown actual mapping function g^* . Therefore, we model our DNN-MUD to thoroughly understand the correlation of the sensing matrix Φ . Mutual coherence is the measure of the correlation between two columns of a matrix which is defined as

$$\zeta(\Phi) = \max_{i \neq j} |\Phi_i^H \Phi_j|. \quad (13)$$

In order to learn the correlation structure of the matrix Φ and to improve the MUD performance, we consider the restricted isometric property (RIP) [28] of the sensing matrix Φ to the design of the architecture. There exists a restricted isometric constant (RIC) $\delta_s \in (0, 1)$ satisfying

$$(1 - \delta_s) \|\varphi\|_2^2 \leq \|\Phi\varphi\|_2^2 \leq (1 + \delta_s) \|\varphi\|_2^2. \quad (14)$$

Hence, a smaller δ_s achieves better MUD performance. Therefore we consider the minimization of RIC by the design of our DNN-MUD architecture.

B. MUD and Sparsity Estimation Architecture for SMV

The proposed DNN-MUD architecture is designed based on the ResNet concept, which has several residual blocks. Each residual block consists of layers and functions such as dense, dropout, rectified linear unit (ReLU) activation unit, batch normalization, $L2$ regularization, and identity connection. DNN learns the parameters during backpropagation by calculating the error and gradient. Based on the gradient value, the weights of the hidden nodes are updated. This process continues until it reaches the input layer. The significant advantage of choosing ResNet over other architectures is to control the vanishing gradients where the identity connection holds it. During the training phase of the DNN-MUD, while learning the codebook parameters, it also learns the residual function. Clearly, DNN learns the difference between the input and the output, improving the system's accuracy until the residual value approaches zero. Therefore introducing the identity connection eases the training and improves the overall performance. Furthermore, the identity connection does not have any weight. Consequently, it does not include any parameters to the network; hence computational complexity remains the same as deep feedforward neural network. In this study, we generate the set \mathcal{D} of D training data $(\tilde{\mathbf{y}}_p^{(1)}, \dots, \tilde{\mathbf{y}}_p^{(D)})$ for each training iteration. Here, $\tilde{\mathbf{y}}_p^{(d)}$ is a complex vector that cannot give direct input to the DNN because our label is not in the complex form. Therefore we split real and imaginary parts separately and stack them as a vector input to the system as

$$\tilde{\mathbf{y}}_p^{(d)} = [\Re(\tilde{y}_p^{(d)}), \dots, \Re(\tilde{y}_p^{(d)}), \Im(\tilde{y}_p^{(d)}), \dots, \Im(\tilde{y}_p^{(d)})]^T. \quad (15)$$

Fig. 2 shows the detailed structure of the proposed ResNet based DNN-MUD. First, the input data passes through the fully connected (FC) layer and the output vector $\tilde{\mathbf{z}}^{(d)} \in \mathbb{R}^{v \times 1}$ of the FC layer is given by

$$\tilde{\mathbf{z}}^{(d)} = \mathbf{W}^{in} \tilde{\mathbf{y}}_p^{(d)} + \mathbf{b}^{in}, \text{ for } d = 1, \dots, D, \quad (16)$$

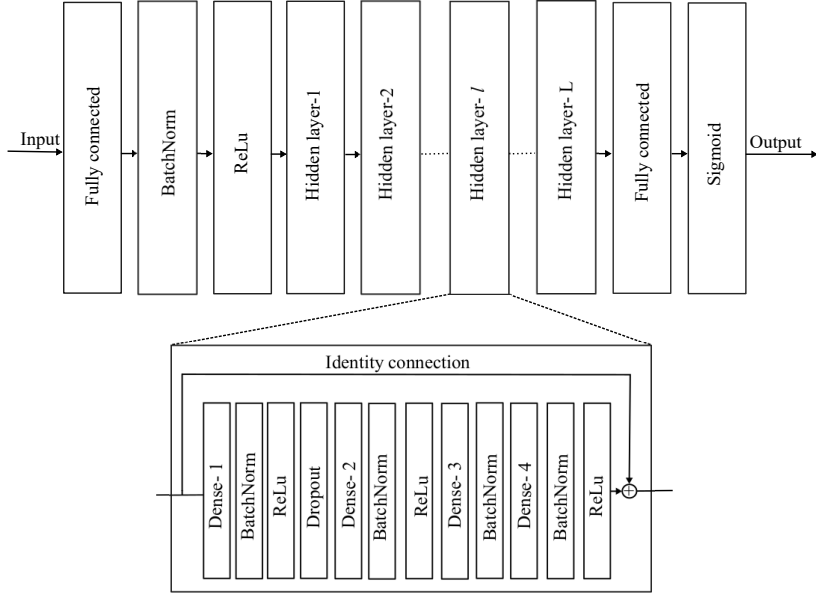


Fig. 2: The complete configuration of the proposed ResNet concept-based MUD, including the layer structure of each hidden layer.

where $\mathbf{W}^{in} \in \mathbb{R}^{v \times 2K}$ is the initial weight, $\mathbf{b}^{in} \in \mathbb{R}^{v \times 1}$ is the initial bias and v is the width of the hidden nodes. After that, D number of resulting vectors are assembled in the mini-batch \mathcal{B} . Then, we add the batch normalization layer, where each element $\tilde{z}_j^{(d)}$ in \mathcal{B} is normalized to have zero-mean and unit-variance. The resulting vector $\hat{\mathbf{z}}^{(d)}$ of the batch normalization layer [29] is stated as

$$\hat{z}_j^{(d)} = \gamma \left(\frac{\tilde{z}_j^{(d)} - \mu_{B,j}}{\sqrt{\sigma_{B,j}^2}} \right) + \eta, \text{ for } j = 1, \dots, v, \quad (17)$$

where γ and η are scaling and shifting parameters, respectively. $\mu_{B,j}$ and $\sigma_{B,j}^2$ are the batch-wise mean and variance, respectively. The function of the normalization layer is to ensure that the input distribution has a fixed mean and variance, which improves the learning of the DNN. Also, larger variances of the training data reduce the learning of the internal features from the input signal. Therefore, batch normalization controls the interpretation affected by the various wireless channels and noise. Then, a nonlinear activation function is applied to the output of the batch normalization layer to determine whether the information passing through the hidden unit is activated. We added the ReLU activation [30] unit before inputting the data to the identity blocks as the nonlinear activation function. The ReLU activation function is expressed by $\sigma(x) =$

$\max(x, 0)$. Therefore the input to the first hidden layer is given by

$$\check{\mathbf{z}}^{(d)} = \sigma(\hat{\mathbf{z}}^{(d)}). \quad (18)$$

After the ReLU activation, the output vector passes through several identical blocks. Every block consists of four dense layers, four batch normalization layers, three ReLU activation units, a dropout layer, and a residual connection. Inside the identical block, the output of the first three layers follows as (16), (17), (18) with corresponding layer parameters. After that, a dropout layer is added to regularize the model to avoid the risk of overfitting and to distinguish the proper support. At the dropout layer, some activated hidden layer output units are randomly dropped out during the training by removing the connectivity of incoming and outgoing layers. The reason is the estimation of the Ω depends on the activation patterns of the hidden units. Furthermore, if the sensing matrix Φ is less correlated (low mutual coherence), then the detection of the active devices would be comparatively straightforward. However, when the number of active devices increases Φ becomes highly correlated, which makes the estimation difficult. In effect, each update to a layer during training is performed with a different perspective of the configured layer. Therefore, the ambiguity of the activation patterns among correlated supports can be improved, which reduces the generalization error in the DNN. We define the dropout vector for the l -th identity block as $\mathbf{q}^{(l)}$, then j -th component $q_j^{(l)}$ of the vector $\mathbf{q}^{(l)}$ can be expressed as

$$q_j^{(l)} = \text{Bernoulli}(P_{dr}), \quad (19)$$

where P_{dr} is the dropout probability of the Bernoulli random variable. In complex DNN models, there is a possibility that the model learns the noise in the training data and performs better during the training phase, but fails to detect during the testing phase where the noise is different. To avoid this, we added another dense layer with $L2$ regularizer after the dropout layer, where the regularizer introduces penalties to the specific layer parameters to avoid high variance. Here, we intend to introduce a decay function to the layer's weights, introducing a summed value to the regular loss function. Therefore, the updated loss function is given by

$$\tilde{\mathcal{L}}(\mathbf{W}_2^l) = \mathcal{L}(\mathbf{W}_2^l) + \frac{\epsilon}{2} \|\mathbf{W}_2^l\|_2^2, \quad (20)$$

where $\mathcal{L}()$ is the loss function, $\mathbf{W}_2^l \in \mathbb{R}^{v \times v}$ is the weights of the second dense layer of the l -th hidden block, and ϵ is the regularization ratio. During the training process, the $L2$ regularizer adds further subtraction on the current weights of the specific layer based on the ϵ value, which further improves the learning quality of the DNN. After that, we continue with the layers mentioned

in Fig. 2. Specifically, we include a ReLU activation at the identity block's end to refine the path from one identical block to another. Therefore activated units are connected to improve the contribution of every identical block in the DNN-MUD. After having gone through all identical hidden layers, the last FC layer produces N output values equal to the total number of MTDs. The output vector is given by

$$\mathbf{z}^{out} = \mathbf{W}^{out} \left(\check{\mathbf{z}}^{(d)} + \sum_{l=1}^L \bar{\mathbf{z}}_l^{(d)} \right) + \mathbf{b}^{out}, \quad (21)$$

where $\bar{\mathbf{z}}_l^{(d)}$ is the output of the hidden block l , $\mathbf{W}^{out} \in \mathbb{R}^{N \times v}$, and $\mathbf{b}^{out} \in \mathbb{R}^{N \times 1}$ are the corresponding weight and bias of the last FC layer, respectively. After that, the sigmoid function produces N independent probabilities $(\hat{p}_1, \dots, \hat{p}_N)$ based on the previous layer. The probability of the j -th MTD being active is given by

$$\hat{p}_j = \frac{1}{1 + e^{-z_j^{out}}}, \text{ for } j = 1, \dots, N. \quad (22)$$

Finally, DNN detects the active devices based on the sigmoid probability. The output estimation is given by

$$\tilde{\Omega} = \arg \max_{|\Omega|=n} \sum_{j \in \Omega} \hat{p}_j. \quad (23)$$

Here, the value of n and their positions solve the previously stated two subproblems. DNN-MUD learns the sparsity by properly annotating training labels during the training phase. Therefore, DNN-MUD satisfies (23) and detects the active MTDs from the test data set.

C. MUD and Sparsity Estimation Architecture for MMV

Given that BSs are not limited by energy and computation complexity constraints, BSs in many practical network deployments are equipped with multiple antennas. We consider BS equipped with a $X > 1$ antennas and MTDs equipped with a single antenna. Accordingly, BS receives multiple measurement vectors for each transmission. Therefore the previously mentioned SMV-based MUD becomes MMV-based MUD. Considering the facts, the received signal at the BS can be written as

$$\mathbf{Y}_p = \Phi \Psi + \mathbf{W}_p, \quad (24)$$

where $\mathbf{Y}_p = [\mathbf{y}_{p,1} \dots \mathbf{y}_{p,X}]$ and $\Psi = [\varphi_1 \dots \varphi_X]$. Here, the set of active MTDs at a given time slot is the same for all X antennas. Therefore, the sparsity of $(\varphi_1 \dots \varphi_X)$ are the same. Hence, the MMV scenario gives additional information about the different channel parameters

to support MUD. Therefore we are only considering changing the input data to our DNN-MUD while the labels remain unchanged. In this subsection, we generate the set $\tilde{\mathcal{D}}$ of D training data $(\tilde{\mathbf{Y}}_p^{(1)}, \dots, \tilde{\mathbf{Y}}_p^{(D)})$ for each training iteration. Here, $\tilde{\mathbf{Y}}_p^{(d)}$ is a complex matrix that cannot input directly into the DNN because our label is not in the complex form. Therefore we split the matrix $\tilde{\mathbf{Y}}_p^{(d)}$ into vectors $(\tilde{\mathbf{y}}_{p,1}^{(d)} \dots \tilde{\mathbf{y}}_{p,X}^{(d)})$ and split each of the vectors in the same way of SMV. We split real and imaginary parts of the vectors separately and stack them according to the antenna order, and create a vector input to the system as

$$\begin{aligned}\hat{\mathbf{y}}_p^{(d)} = & [\{\Re(\tilde{y}_{p,1,1}^{(d)}), \dots, \Re(\tilde{y}_{p,1,K}^{(d)}), \Im(\tilde{y}_{p,1,1}^{(d)}), \dots, \Im(\tilde{y}_{p,1,K}^{(d)})\}, \\ & \dots, \{\Re(\tilde{y}_{p,X,1}^{(d)}), \dots, \Re(\tilde{y}_{p,X,K}^{(d)}), \Im(\tilde{y}_{p,X,1}^{(d)}), \dots, \Im(\tilde{y}_{p,X,K}^{(d)})\}]^T.\end{aligned}\quad (25)$$

After that, we use the same architecture as the SMV mentioned in Fig. 2 to support the MMV scenario with different layer parameters. In MMV, we have X -fold increase in the training data for the same label, which leads to improved MUD with the lower training overhead for the same performance level.

IV. THEORETICAL ANALYSIS FOR COMPLEXITY AND IMPLEMENTATION

A. Complexity Analysis

It is necessary to investigate the computational complexity of the proposed DNN-MUD to examine the practical feasibility of the algorithm in mMTC networks. In this regard, we calculate the floating-point operations (FLOPs), which include all floating-point operations of the FC layer, batch normalization layer, activation functions, dropout, and sigmoid function. First, FLOPs of the initial FC layer (16), which include matrix multiplication of $\mathbf{W}^{in} \in \mathbb{R}^{v \times 2K}$ with $\tilde{\mathbf{y}}_p^{(d)} \in \mathbb{R}^{2K \times 1}$ and a vector addition of $\mathbf{b}^{in} \in \mathbb{R}^{v \times 1}$ is given as

$$\mathcal{S}_1 = (4K - 1)v + v. \quad (26)$$

Second, FLOPs of bath normalization layer (17), which involves element-wise addition, element-wise multiplication, scaling, and shifting, is given by

$$\mathcal{S}_2 = 4v. \quad (27)$$

Then, FLOPs of the pre-activation ReLU unit is stated as

$$\mathcal{S}_3 = v. \quad (28)$$

TABLE I: Computational Complexity

Algorithm	DNN-MUD	stOMP	LS-BOMP	C-AMP
Complexity	$\mathcal{O}(Lv^2)$	$\mathcal{O}(N \log N)$	$\mathcal{O}(nK^2N)$	$\mathcal{O}(NK\tau)$

Next, there are L hidden layers involved in the design. Each hidden layer contains four dense layers, four batch normalization layers, three ReLU activation units, a dropout layer (FLOPs = v), and a identity connection (FLOPs = v). Therefore, the total FLOPs of hidden layers are defined by

$$\mathcal{S}_4 = L \left(4[(2v-1)v + v] + 4(4v) + 3v + v + v \right). \quad (29)$$

Also, the FLOPs of the final FC layer with $\mathbf{W}^{out} \in \mathbb{R}^{N \times v}$ and $\mathbf{b}^{out} \in \mathbb{R}^{N \times 1}$ is given as

$$\mathcal{S}_5 = (2v-1)N + N. \quad (30)$$

Finally, the FLOPs of the sigmoid layer (22), which contains four separate operations, is defined by

$$\mathcal{S}_6 = 4N. \quad (31)$$

Collectively, the computational complexity of the proposed DNN-MUD (From (26) to (31)) in FLOPs is derived as

$$\begin{aligned} \mathcal{S}_{DNN} &= 8Lv^2 + (21L + 4K + 2N + 5)v + 4N \\ &= \mathcal{O}(Lv^2) \end{aligned} \quad (32)$$

We further investigate the computational complexity of stOMP [23], [31], LS-BOMP [18], and C-AMP [22], [32] algorithms. The complexities in FLOPs are presented in Table I. In addition, τ is the number of iterations in the C-AMP algorithm. We compare the computational complexities in Table I, it is clear that the complexity of the DNN-MUD depends on the internal parameters of the DNN while stOMP, LS-BOMP, and C-AMP rely on the system parameters. Therefore, it is obvious that using DNN algorithms in the mMTC systems is feasible and practical. Furthermore, the complexity of the DNN-MUD is significantly smaller than LS-BOMP and C-AMP algorithms.

B. Training Data Generation and Implementation

The proposed DNN-MUD is supervised learning, more specifically a multi-label classification problem that takes the labeled data as input and learns the mapping between the data and the

corresponding labels. The well-trained and calibrated model can detect the new set of data labels. Therefore, a sufficient amount of training data is required for the convergence of the DNN model. We validate the adequate amount of data by the loss function of the DNN model. The proposed model can learn the codebook parameters from the actual received signal. However, we can train, validate, and test the DNN using synthetically generated data. The industrial application can directly feed the received signal with proper labels to the DNN model, which is feasible since this application is for uplink communication of mMTC.

In the generated data, the received signal contains the sparse input vector φ and the sensing matrix Φ where all environment channel properties and randomness are involved in the sparse vector, not in the sensing matrix. The core learning component of the DNN depends on the codebook for SCMA and spreading sequences for MUSA, which is known to the BS a priori. Hence, the synthetically generated data does not degrade the performance of the proposed DNN-MUD. Consequently, we generate the SCMA codebook and MUSA spreading sequences for the different simulation requirements. Then, create the channel vector and random noise vector w . Finally, the training data is produced using (3), and the sparse block vector's support is used as the training label. Furthermore, we train the DNN-MUD model offline for various environmental conditions with a different number of MTDs and a random number of active devices. Hence, re-training of the model is unnecessary unless new devices are added.

V. SIMULATION RESULTS

We explore the performances of the proposed DNN-MUD for SCMA and MUSA systems in this section. CSI is not assumed at the BS since the BS does not know the active users a priori and cannot extract the CSI from the pilot sequences. First, we show the results of the system performances of the DNN to ensure correctness and reliability. Then, we present the outcomes for the SMV scenario in comparison with LS-BOMP [21], C-AMP [22], and stOMP [22]. The LS-BOMP minimizes the least-squares of a linear system with ℓ_0 constraint and estimates the active devices with the knowledge of sparsity, C-AMP uses state evolution to estimate the active devices without the knowledge of sparsity, and stOMP evaluates the sparsity by sequentially transforming the received signal into a negligible residual in a fixed number of stages with the knowledge of the sparsity. After that, we demonstrate the plots of the MMV scenario. Finally, MUD results for the four different mmWave indoor factory environments are presented. The simulation parameters for the first four subsections are presented in Table II.

TABLE II: Simulation Parameters

Parameter	Value
Overloading ratios (OR)	150%, 300%
Number of MTDs in SCMA (N)	90
Number of MTDs in MUSA (N)	21
Active probability (p_i)	$1/N$
MTD to BS path loss model	$128.1 + 37.6 \log_{10}(r_i[Km])$
Log-normal shadow fading	8 dB
Noise spectral density	-174 dBm/Hz
Transmission bandwidth	1 MHz
Noise figure at BS	4 dB
DNN sample size	10^6
Number of hidden layers (L)	4
Learning rate	1×10^{-3}
Batch size	1×10^3
Epoch	50
Drop out, P_{dr}	0.5

We use the binary cross-entropy as the loss function and the Adam optimizer to guarantee the model's convergence. The proposed DNN-MUD was designed, trained, validated, and tested on Keras with the Tensorflow backend. For the performance matrices, we use true positives (tp), and true negatives (tn), false positives (fp), and false negatives (fn), and area under the curve (AUC) to train and validate the proposed DNN-MUD model. Then, we examine the probability of detection (recall) on the testing set as $(P_D) = (\frac{tp}{tp+fn})$, probability of misdetection (false negative rate) as $(P_M) = (\frac{fn}{tp+fn})$, positive predictive values (precision) = $(\frac{tp}{tp+fp})$, and binary accuracy = $(\frac{tp+tn}{tp+fb+tn+fn})$ to ensure the correctness of the probability of detection.

A. Performance of MUSA sequence selection algorithm

First, we consider the performance of the proposed MUSA sequence selection algorithm by plotting the correlation among the selected codewords. Fig. 3 compares the correlation of the MUSA sequences selected by the proposed Algorithm 1 (Fig. 3a) against a random selection of MUSA sequences from the available set (Fig. 3b). The proposed algorithm shows a high degree of auto-correlation and low cross-correlation for the selected MUSA sequences as it chooses

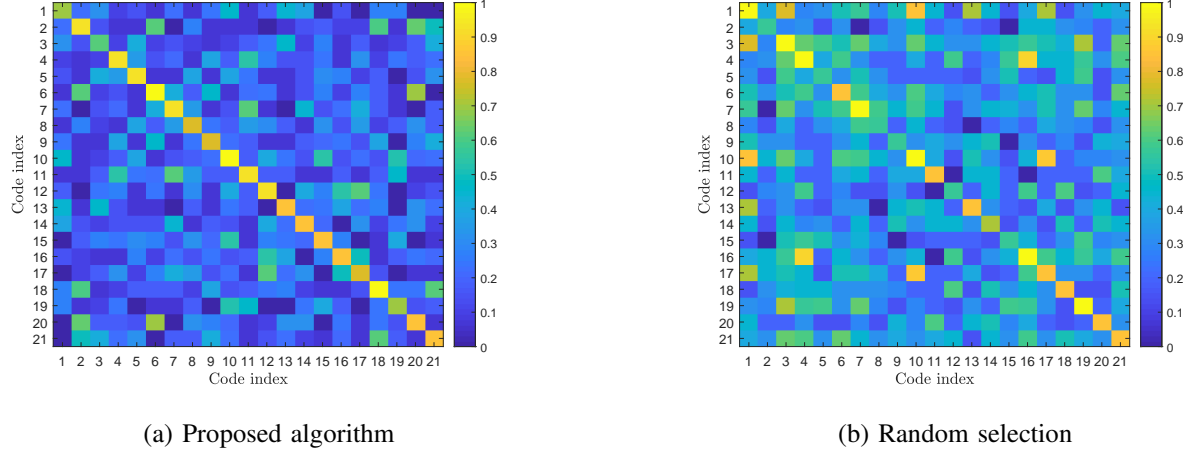


Fig. 3: Correlation of the MUSA sequences (a) selection by the proposed Algorithm 1 and (b) random selection.

the sequences based on the orthogonality threshold value. In comparison, the randomly selected MUSA sequences do not exhibit a similar level of orthogonality.

B. System Performance of DNN

We evaluate the performance of the DNN-MUD with the perfect detection of active devices. Fig. 4a and Fig. 4b show the calibration curve for the SCMA and MUSA systems, respectively. The calibration curve compares the expected output and the predicted output of the system. Furthermore, it is one of the standard approaches to evaluating system performance in multi-label classification. Our calibration curve clearly shows the perfectness of the DNN-MUD for OR = 150%. In contrast, the requirement for the specific mechanism to improve the detection performance at higher ORs like 300% which we discussed in subsection D.

C. MUD for the SMV Scenario

First, we study the probability of detection of the proposed DNN for both SCMA and MUSA systems and show the result in Fig. 5. We observe that DNN-MUD outperforms the stOMP, LS-BOMP, and C-AMP algorithms for both SCMA and MUSA systems even though the OR increases from 150% to 300%. In MUSA systems, stOMP is able to detect active devices to a certain extent with known sparsity, nevertheless unable to defeat the DNN-MUD.

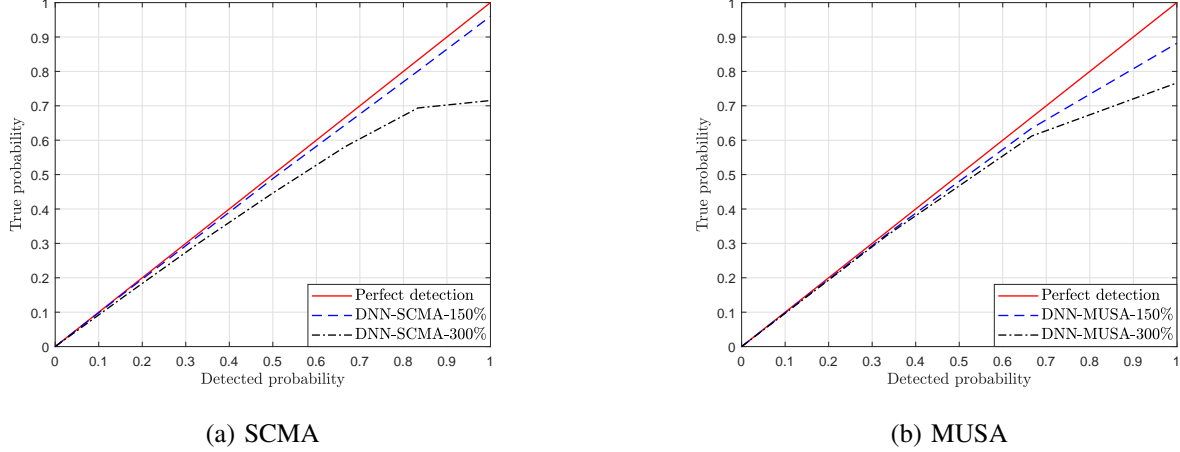


Fig. 4: Calibration curve for DNN-MUD for both SCMA and MUSA systems with two different ORs (SNR = 20 dB, $X = 1$).

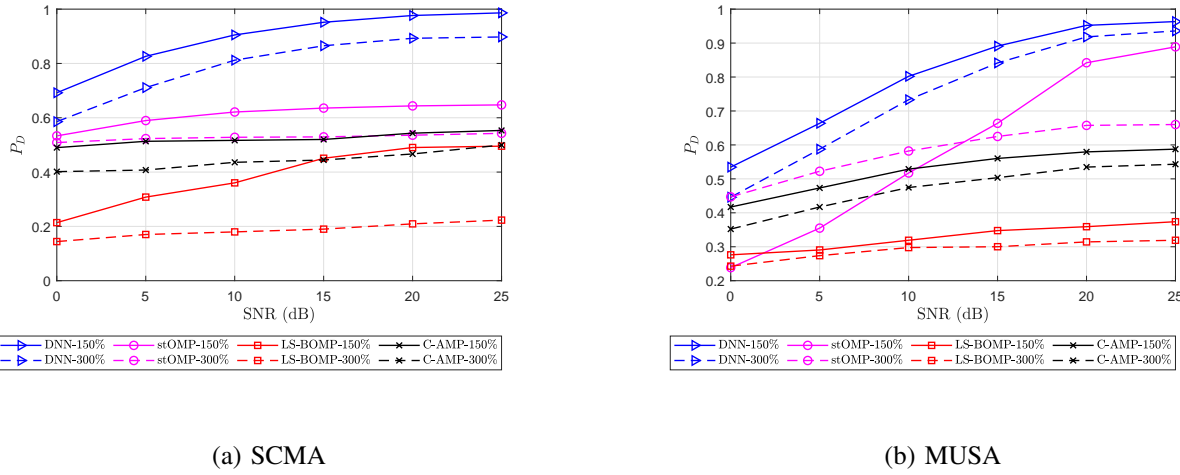


Fig. 5: Probability of detection (recall) versus the SNR for four different MUD schemes for (a) the SCMA codebook ($N = 90$, $X = 1$, $n = 3$) and (b) the MUSA spreading sequences ($N = 21$, $X = 1$, $n = 2$) with two different overloading ratios.

We evaluate precision, binary accuracy, and AUC apart from the recall value to ensure the trustworthiness of the DNN and plot the results for the SCMA and MUSA system in Fig. 6 and Fig. 7, respectively. Combining the outcomes of Fig. 5 with Fig. 6a and Fig. 7a, we understand the reliability of the DNN regarding the type-I (false positive) and type-II (false negative) errors. Furthermore, the binary accuracy of both SCMA and MUSA systems under

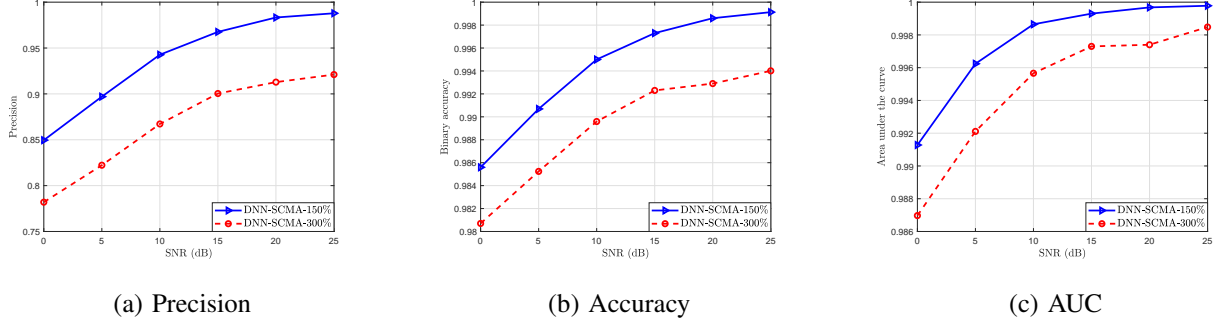


Fig. 6: DNN performance matrices for the SCMA scenario ($N = 90$, $X = 1$, $n = 3$).

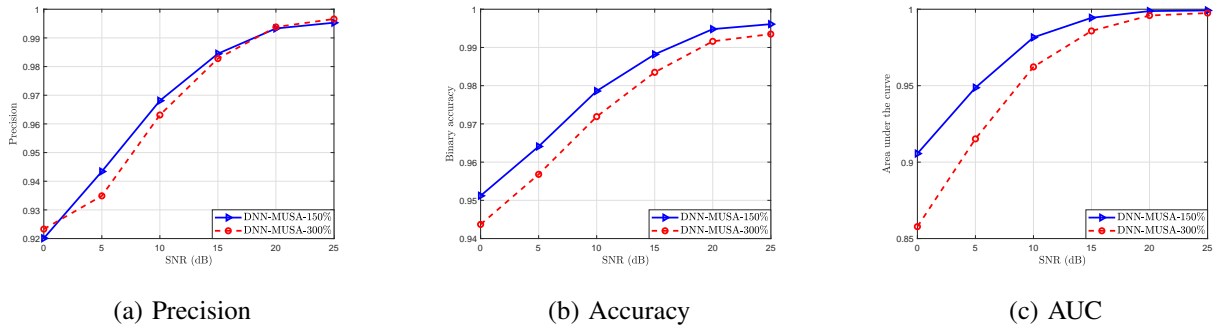


Fig. 7: DNN performance matrices for MUSA scenario ($N = 21$, $X = 1$, $n = 2$).

two different ORs beyond 94% indicates the overall performance. Likewise, the AUC reaches 1 when SNR increases, which indicates the detection accuracy of our proposed approaches.

Second, we explore the probability of detection versus the number of active MTDs at SNR = 20 dB. We observe that the DNN-MUD is superior to its counterparts in the entire region. Specifically, the examination was carried up to 10% and 30% of active devices out of all devices in SCMA and MUSA systems, respectively. Regardless, mMTC requirement of active devices is around 5% to 10% of total devices in a time frame. Furthermore, we can observe that the likelihood of detecting stOMP is around 50% and C-AMP is around 47% for OR = 150% in SCMA systems while DNN reaches more than 95%. We can see the robustness of the DNN-MUD scheme with an increased number of active devices. According to the present results, when n increases, the mutual coherence of the system rises sharply, leading to performance degradation. However, the DNN-MUD can handle this subject by learning the sensing matrix during the training phase, while stOMP, LS-BOMP, and C-AMP do not.

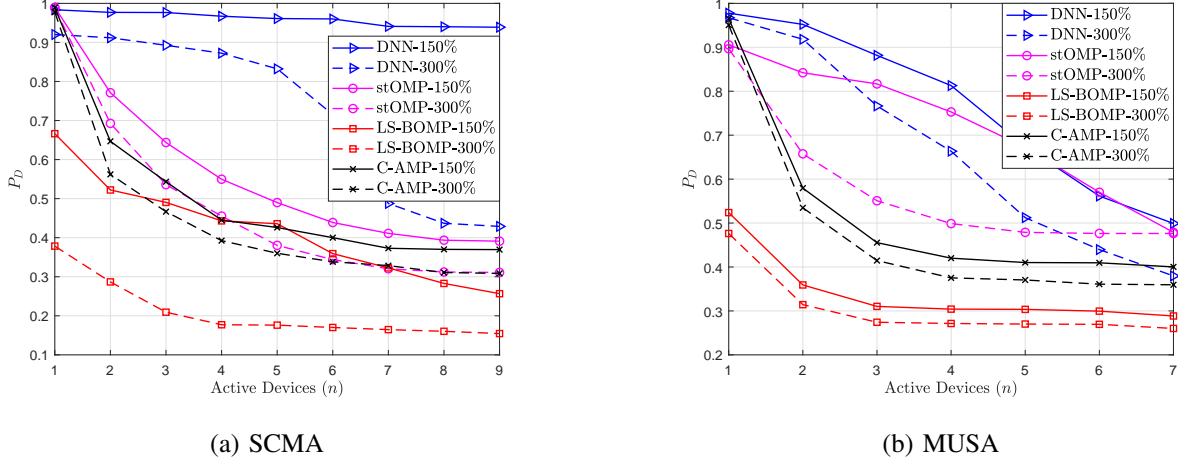


Fig. 8: Probability of detection (recall) versus the device activity for four different MUD schemes for (a) the SCMA codebook ($N = 90$, $X = 1$) and (b) the MUSA spreading sequences ($N = 21$, $X = 1$) with two different overloading ratios when $\text{SNR} = 20$ dB.

Finally, we investigate the probability of misdetection (false-negative rate) versus the number of active devices at $\text{SNR} = 20$ dB for DNN-MUD compared to stOMP, LS-BOMP, and C-AMP algorithms which are presented in Fig. 9. This outcome clearly explains that even though the number of active devices increases, the false-negative rate does not defeat by other algorithms for SCMA and MUSA systems under different OR scenarios. For example, there are 164 misdetections out of 10^4 samples when $n = 1$ while there are 611 misdetections out of 10^4 samples when $n = 9$ for SCMA codebooks with 150% ORs.

D. MUD for the MMV Scenario

Next, we evaluate the performance of DNN-MUD for MMV systems. Fig. 9 presents the variation of the probability of detection versus SNR with three different antenna configurations for both SCMA and MUSA systems; when X increases, the spatial diversity increases, improving the detection probability. For example, at $\text{SNR} = 10$ dB the probability of detection improves from 81% to 97% when X changes from $X = 1$ to $X = 2$ for SCMA codebooks with 300% OR. Likewise, for MUSA spreading sequences with 300% OR, the performance improves from 73% to 92%. Moreover, the probability of detection reaches 100% for both SCMA and MUSA systems with 150% and 300% ORs, when X goes to $X = 4$ at $\text{SNR} = 15$ dB.

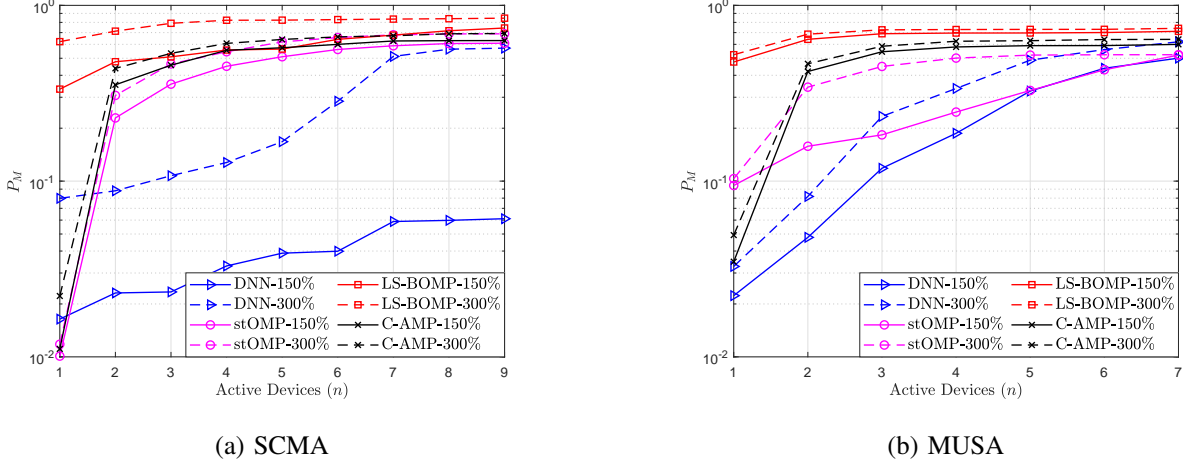


Fig. 9: Probability of misdetection versus the device activity for four different MUD schemes for (a) the SCMA codebook ($N = 90$, $X = 1$) and (b) the MUSA spreading sequences ($N = 21$, $X = 1$) with two different overloading ratios when $\text{SNR} = 20$ dB.

Here, we design our DNN such that with twice the number of input neurons when X increases from one to two and two to four to achieve the advantage of the spatial diversity of the MMV system. Furthermore, the increased input neurons improve the learning capability of the DNN. Notably, the MMV system is the proactive solution to the issue we observed and discussed in Fig. 4 for higher OR ratios. Based on the outcomes, we can state that increasing the number of antennas at the BS is ideal for overcoming the drawbacks of higher ORs of SCMA and MUSA systems, which are applicable in mMTC for future wireless communication requirements.

E. MUD for the mmWave Indoor Factory Environment

In this subsection, we consider the next-generation mMTC application environment. 5G NR spectrum includes the 26 GHz mmWave band, while IEEE 802.11 ad/ay is defined for the 60 GHz band (known as WiGig or 60 GHz Wi-Fi). Future beyond 5G/6G wireless networks are expected to operate at even higher frequency bands [3]. Thus, there is a requirement to investigate high-frequency channel models. In that respect, we propose the SMV DNN MUD problem for mmWave channel models based on the 3GPP specifications. We consider the indoor factory (InF) environment with various sizes and various density levels of machinery. 3GPP proposes five types of channel models for InF, first is sparse clutter with low BS height (InF-SL), second is dense clutter with low BS height (InF-DL), third is sparse clutter with high BS height (InF-

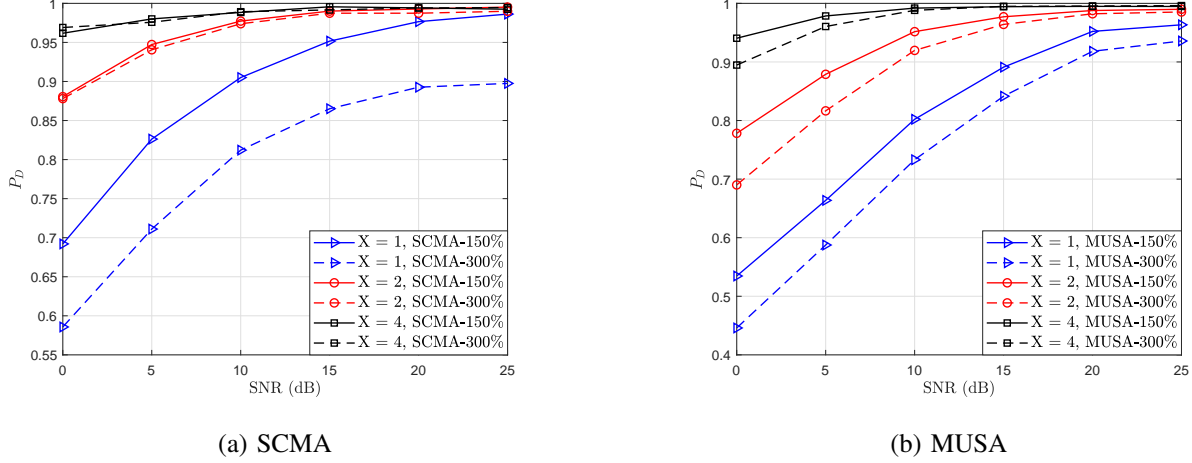


Fig. 10: Probability of detection (recall) versus the SNR for two different overloading ratios for (a) SCMA codebooks ($N = 90$, $n = 3$) and (b) MUSA spreading sequences ($N = 21$, $n = 2$) with three different number of antenna configurations.

SH), fourth is dense clutter with high BS height (InF-DH), and the fifth is for 100% line of sight (LOS) scenario [24]. We choose the first four categories for further study. Furthermore, the sparse clutter environment consists of large metallic machinery placed inside the factory with sufficient clearance between the big machines with a considerable amount of open space available. Meanwhile, the dense clutter scenario contains the small and medium size of metallic irregular types of machinery.

In all four InF scenarios, we consider the line of sight (LOS) and non-LOS (NLOS) based on the LOS probabilities defined by 3GPP [24]. In accordance, the 3D distance r_{3D} between BS and the MTD is given as

$$r_{3D} = \sqrt{r_{2D}^2 + (h_{BS} - h_{MTD})^2}, \quad (33)$$

where r_{2D} is the 2D distance between the BS and the MTD, h_{BS} is the height of the indoor BS, and h_{MTD} is the height of the location where the MTD is deployed. The LOS pathloss of the all four InF scenarios define as

$$PL_{LOS} = 31.84 + 21.50 \log_{10}(r_{3D}) + 19.00 \log_{10}(f_c) + \chi_{\sigma_{LOS}}, \quad (34)$$

where f_c is the normalized carrier frequency and with the corresponding shadow fading standard deviation $\sigma_{LOS} = 4.3$. The NLOS pathloss define as

$$PL = a + b \log_{10}(r_{3D}) + 20.00 \log_{10}(f_c) + \chi_{\sigma_{NLOS}}, \quad (35)$$

TABLE III: InF environment parameters

InF scenario	h_{BS}	h_{MTD}	ς	h_c	r_c	$r_{2D\text{range}}$	a	b	σ_{NLOS}
InF-SL	1.5 m	1.5 m	20%	2 m	10 m	25 – 200 m	33.00	25.50	5.70
InF-DL	1.5 m	1.5 m	60%	6 m	2 m	18 – 108 m	18.60	35.70	7.20
InF-SH	8.0 m	1.5 m	20%	2 m	10 m	40 – 488 m	32.40	23.00	5.90
InF-DH	8.0 m	1.5 m	60%	6 m	2 m	24 – 420 m	33.63	21.90	4.00

$$PL_{NLOS} = \max(PL_{LOS}, PL), \quad (36)$$

where values of a and b varies with different InF scenarios. The values of a , b , and shadow fading standard deviations σ_{NLOS} are given in Table III. The LOS probabilities of all four InF scenarios define as

$$Pr_{LOS} = \exp\left(-\frac{r_{2D}}{k_s}\right), \quad (37)$$

where k_s given by

$$k_s = \begin{cases} -\frac{r_c}{\ln(1-\varsigma)}, & \text{for InF-SL and InF-DL,} \\ -\frac{r_c}{\ln(1-\varsigma)} \cdot \frac{h_{BS}-h_{MTD}}{h_c-h_{MTD}}, & \text{for InF-SH and InF-DH,} \end{cases} \quad (38)$$

where r_c is the clutter size, ς is the clutter density, and h_c is the effective clutter height. We train our model for all four types of InF scenarios to detect the active MTDs. InF environment parameters are presented in Table III. Here, we define different r_{2D} ranges for all InF scenarios to compare the performances in specific SNR values while maintaining the channel model condition that, $1 \leq r_{3D} \leq 600$ m given in [24]. Furthermore, we used the same ORs, N in both SCMA and MUSA, p_i , noise spectral density, noise figure at BS, and DNN parameters same as the Table II. In addition, we consider $f_c = 28$ GHz and transmission bandwidth 100 MHz for the mmWave InF simulations.

Finally, we simulate the four different InF environments and evaluate the performance of the DNN MUD for the SMV system to verify the algorithm's applicability in future smart factories. Fig. 11 presents the probability of detection versus SNR for InF-SL, InF-SH, InF-DL, and InF-DH. Here, we observe that InF-DH achieves the highest overall performance in both SCMA and MUSA scenarios because of the higher chance of the LOS probability. Also, due to the ς difference between InF-DH and InF-SH, InF-SH reaches the second-highest overall performance. Likewise, the performance of InF-DL and InF-SL follows the argument as mentioned earlier.

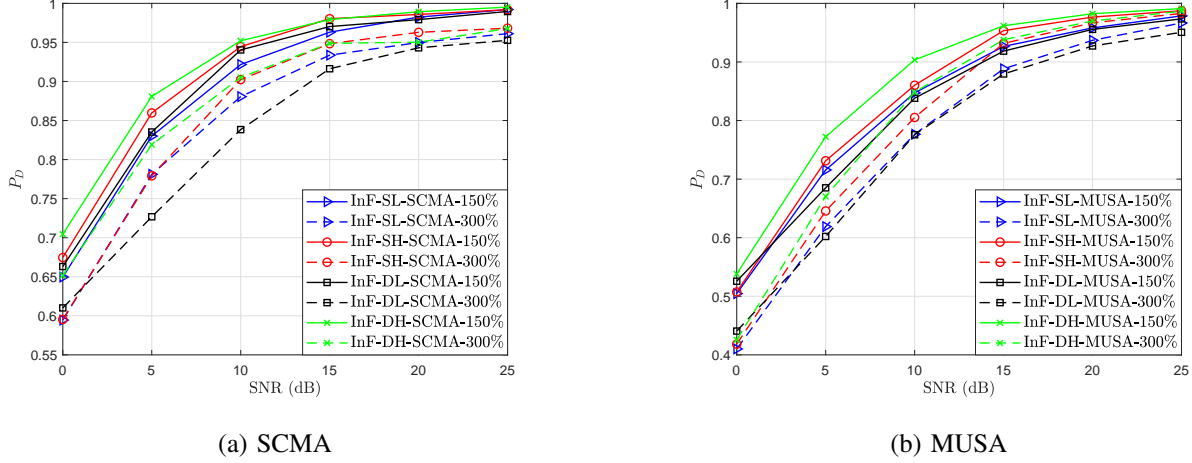


Fig. 11: Probability of detection (recall) versus the SNR for two different overloading ratios for (a) SCMA codebooks ($N = 90$, $n = 3$) and (b) MUSA spreading sequences ($N = 21$, $n = 2$) with four different number of indoor factory environments.

VI. CONCLUSION

In this paper, we have considered jointly detecting the sparsity of the received signal and corresponding active devices in two different grant-free NOMA mMTC systems in the absence of CSI at the BS. The main motivation is to blindly detect active devices in SMV and MMV systems with diverse ORs and explore the performance in a mmWave system setting with lower computational complexity. We have proposed a pre-activated ResNet-based DNN-MUD architecture to address the challenging sparse signal recovery problem. For the detailed examination of the proposed DNN-MUD, we have included an SCMA codebook design for a large number of devices and MUSA spreading sequence generation with a scalable heuristic algorithm to determine the spreading sequences. Furthermore, we have presented complete architecture details, including pre-activation, hidden layer design, post-activation, dropout, regularization, choice of the loss function, training data generation, and label annotation. In numerical simulations, we have carried out the system performance of the DNN-MUD to validate the effectiveness of the proposed architecture. The performance of the proposed DNN-MUD scheme is comprehensively analyzed and is found to outperform well-known existing MUD algorithms. Simulation results of the SMV have shown that using DNN-MUD to detect the active MTD is a perfect choice even when the device activity level is high in a single time frame. Moreover, MMV systems

have shown a very high probability of detection performance regardless of OR of the codes. The low computational complexity of the DNN-MUD further highlights the significance of the proposed approach, which encourages the less complex DNN powered architectures for future mMTC applications.

REFERENCES

- [1] T. Sivalingam, S. Ali, N. H. Mahmood, N. Rajatheva, and M. Latva-Aho, “Deep learning-based active user detection for grant-free SCMA systems,” in *2021 IEEE 32nd Annual International Symposium on Personal, Indoor and Mobile Radio Communications (PIMRC)*, 2021, pp. 635–641.
- [2] T. Sivalingam, S. Ali, N. Huda Mahmood, N. Rajatheva, and M. Latva-Aho, “Deep neural network-based blind multiple user detection for grant-free multi-user shared access,” in *2021 IEEE 32nd Annual International Symposium on Personal, Indoor and Mobile Radio Communications (PIMRC)*, 2021, pp. 1–7.
- [3] N. Rajatheva, I. Atzeni, E. Björnson, A. Bourdoux *et al.*, *White Paper on Broadband Connectivity in 6G*, ser. 6G Research Visions, nr. 10, N. Rajatheva, Ed. Oulu, Finland: University of Oulu, Jun. 2020, white Paper. [Online]. Available: <http://jultika.oulu.fi/files/isbn9789526226798.pdf>
- [4] S. Ali, N. Rajatheva, and W. Saad, “Fast uplink grant for machine type communications: Challenges and opportunities,” *IEEE Communications Magazine*, vol. 57, no. 3, pp. 97–103, 2019.
- [5] M. Hasan, E. Hossain, and D. Niyato, “Random access for machine-to-machine communication in LTE-advanced networks: Issues and approaches,” *IEEE Communications Magazine*, vol. 51, no. 6, pp. 86–93, 2013.
- [6] L. Dai, B. Wang, Y. Yuan, S. Han, I. Chih-lin, and Z. Wang, “Non-orthogonal multiple access for 5G: solutions, challenges, opportunities, and future research trends,” *IEEE Communications Magazine*, vol. 53, no. 9, pp. 74–81, 2015.
- [7] M. Mohammadkarimi, M. A. Raza, and O. A. Dobre, “Signature-based nonorthogonal massive multiple access for future wireless networks: Uplink massive connectivity for machine-type communications,” *IEEE Vehicular Technology Magazine*, vol. 13, no. 4, pp. 40–50, 2018.
- [8] M. Taherzadeh, H. Nikopour, A. Bayesteh, and H. Baligh, “SCMA codebook design,” in *2014 IEEE 80th Vehicular Technology Conference (VTC2014-Fall)*, 2014, pp. 1–5.
- [9] Z. Yuan, G. Yu, W. Li, Y. Yuan, X. Wang, and J. Xu, “Multi-user shared access for internet of things,” in *2016 IEEE 83rd Vehicular Technology Conference (VTC Spring)*, 2016, pp. 1–5.
- [10] B. K. Jeong, B. Shim, and K. B. Lee, “MAP-based active user and data detection for massive machine-type communications,” *IEEE Transactions on Vehicular Technology*, vol. 67, no. 9, pp. 8481–8494, 2018.
- [11] M. Ke, Z. Gao, Y. Wu, X. Gao, and R. Schober, “Compressive sensing-based adaptive active user detection and channel estimation: Massive access meets massive MIMO,” *IEEE Transactions on Signal Processing*, vol. 68, pp. 764–779, 2020.
- [12] B. Wang, L. Dai, T. Mir, and Z. Wang, “Joint user activity and data detection based on structured compressive sensing for NOMA,” *IEEE Communications Letters*, vol. 20, no. 7, pp. 1473–1476, 2016.
- [13] Y. Du, B. Dong, Z. Chen, X. Wang, Z. Liu, P. Gao, and S. Li, “Efficient multi-user detection for uplink grant-free NOMA: Prior-information aided adaptive compressive sensing perspective,” *IEEE Journal on Selected Areas in Communications*, vol. 35, no. 12, pp. 2812–2828, 2017.
- [14] B. Wang, L. Dai, Y. Zhang, T. Mir, and J. Li, “Dynamic compressive sensing-based multi-user detection for uplink grant-free NOMA,” *IEEE Communications Letters*, vol. 20, no. 11, pp. 2320–2323, 2016.

- [15] A. Bayesteh, E. Yi, H. Nikopour, and H. Baligh, "Blind detection of SCMA for uplink grant-free multiple-access," in *2014 11th International Symposium on Wireless Communications Systems (ISWCS)*, 2014, pp. 853–857.
- [16] Z. Yuan, C. Yan, Y. Yuan, and W. Li, "Blind multiple user detection for grant-free MUSA without reference signal," in *2017 IEEE 86th Vehicular Technology Conference (VTC-Fall)*, 2017, pp. 1–5.
- [17] S. Ali, W. Saad, N. Rajatheva, K. Chang *et al.*, *White paper on machine learning in 6G wireless communication networks*, ser. 6G Research Visions, nr. 7, S. Ali, Ed. Oulu, Finland: University of Oulu, Jun. 2020, white Paper. [Online]. Available: <http://jultika.oulu.fi/files/isbn9789526226736.pdf>
- [18] W. Kim, Y. Ahn, and B. Shim, "Deep neural network-based active user detection for grant-free NOMA systems," *IEEE Transactions on Communications*, vol. 68, no. 4, pp. 2143–2155, 2020.
- [19] Y. Ahn, W. Kim, and B. Shim, "Deep neural network-based joint active user detection and channel estimation for mMTC," in *ICC 2020 - 2020 IEEE International Conference on Communications (ICC)*, 2020, pp. 1–6.
- [20] D. Cai, P. Fan, X. Lei, Y. Liu, and D. Chen, "Multi-dimensional SCMA codebook design based on constellation rotation and interleaving," in *2016 IEEE 83rd Vehicular Technology Conference (VTC Spring)*, 2016, pp. 1–5.
- [21] H. Li and J. Wen, "A new analysis for support recovery with block orthogonal matching pursuit," *IEEE Signal Processing Letters*, vol. 26, no. 2, pp. 247–251, 2019.
- [22] A. Maleki, L. Anitori, Z. Yang, and R. G. Baraniuk, "Asymptotic analysis of complex LASSO via complex approximate message passing (CAMP)," *IEEE Transactions on Information Theory*, vol. 59, no. 7, pp. 4290–4308, 2013.
- [23] D. L. Donoho, Y. Tsaig, I. Drori, and J.-L. Starck, "Sparse solution of underdetermined systems of linear equations by stagewise orthogonal matching pursuit," *IEEE Transactions on Information Theory*, vol. 58, no. 2, pp. 1094–1121, 2012.
- [24] 3GPP, "5G; Study on channel model for frequencies from 0.5 to 100 GHz," 3rd Generation Partnership Project (3GPP), Technical Report (TR) ETSI TR 138 901 V16.1.0, 11 2020.
- [25] G. Forney and L.-F. Wei, "Multidimensional constellations. i. introduction, figures of merit, and generalized cross constellations," *IEEE Journal on Selected Areas in Communications*, vol. 7, no. 6, pp. 877–892, 1989.
- [26] L. Li, Z. Ma, P. Z. Fan, and L. Hanzo, "High-dimensional codebook design for the SCMA down link," *IEEE Transactions on Vehicular Technology*, vol. 67, no. 10, pp. 10 118–10 122, 2018.
- [27] J. van de Beek and B. M. Popovic, "Multiple access with low-density signatures," in *GLOBECOM 2009 - 2009 IEEE Global Telecommunications Conference*, 2009, pp. 1–6.
- [28] E. J. Candes and T. Tao, "Decoding by linear programming," *IEEE Transactions on Information Theory*, vol. 51, no. 12, pp. 4203–4215, 2005.
- [29] S. Ioffe and C. Szegedy, "Batch normalization: Accelerating deep network training by reducing internal covariate shift," in *Proceedings of the 32nd International Conference on Machine Learning*, ser. Proceedings of Machine Learning Research, F. Bach and D. Blei, Eds., vol. 37. Lille, France: PMLR, 07–09 Jul 2015, pp. 448–456.
- [30] V. Nair and G. E. Hinton, "Rectified linear units improve restricted boltzmann machines," in *Proceedings of the 27th International Conference on International Conference on Machine Learning*, ser. ICML'10. Madison, WI, USA: Omnipress, 2010, p. 807–814.
- [31] S. Qaisar, R. M. Bilal, W. Iqbal, M. Naureen, and S. Lee, "Compressive sensing: From theory to applications, a survey," *Journal of Communications and Networks*, vol. 15, no. 5, pp. 443–456, 2013.
- [32] S. Lyu and C. Ling, "Hybrid vector perturbation precoding: The blessing of approximate message passing," *IEEE Transactions on Signal Processing*, vol. 67, no. 1, pp. 178–193, 2019.